Transport and Defect Mechanisms in Cuprous Delafossites. 1. Comparison of Hydrothermal and Standard Solid-State Synthesis in $CuAlO_2$

Brian J. Ingram, Gabriela B. González,† and Thomas O. Mason*

Department of Materials Science and Engineering and Materials Research Center, Northwestern University, Evanston, Illinois 60208

Dean Y. Shahriari, Antoine Barnabè,§ Donggeun Ko,‡ and Kenneth R. Poeppelmeier

Department of Chemistry and Materials Research Center, Northwestern University, Evanston, Illinois 60208

Received June 25, 2004. Revised Manuscript Received October 1, 2004

$CuAlO_2$ exhibits a unique defect structure that is dependent on the synthesis route. High-temperature solid-state and low-temperature hydrothermal techniques are compared to illustrate how cation off-stoichiometry affects the electrical properties of $CuAlO_2$. A defect complex of Al on a Cu-site stabilized by two bound oxygen interstitials ($Al_{Cu}^{\bullet\bullet}2O_i''$)″ is proposed which serves as an acceptor dopant to set the hole concentration. Trapping of holes (small polarons) by such complexes with decreasing temperature is proposed to account for the decreasing carrier content with temperature. Hydrothermal samples exhibit approximately an order of magnitude increase in hole concentration relative to the solid-state synthesized samples; this is reflected in the electrical conductivity and may explain the variations in electrical properties reported for $CuAlO_2$.

Introduction

Transparent conducting oxides (TCOs) simultaneously exhibit both high transparency through the visible spectrum and high electrical conductivity, which are typically mutually exclusive materials properties. N-type TCOs are utilized in a variety of commercial applications, such as flat-panel displays, photovoltaic devices, and electrochromic windows, in which they serve as transparent electrodes. At the present time there are no commercially viable p-type TCOs. The development of a high figure-of-merit p-type TCO would enable improved flat-panel displays, ultraviolet light emitting diodes, heterojunctions for solar cells, and all-oxide (transparent) semiconductor devices such as diodes and transistors.

Owing to the strong ionic nature of metal−oxygen bonding, holes are typically localized at the valence band edge, which is dominated by oxygen-2p levels therefore limiting p-type conduction. Two methods have been suggested to enhance the covalency between metal−oxygen bonding, thereby limiting localization:[1] choosing cations having closed d-shells of energy comparable to that of the oxygen-2p levels (i.e., Cu^+, Ag^+, and Au^+, especially when found in linear coordination with oxygen[2]), and choosing a structure in which oxygen adopts tetrahedral coordination. An aggressive search for a viable p-type TCO was motivated by the report by Kawazoe et al.[2] of the optical and electrical properties of copper aluminate ($CuAlO_2$) thin films prepared by laser ablation. $CuAlO_2$, which crystallizes in the delafossite structure having the general formula $A^{1+}B^{3+}O_2$, satisfies both conditions facilitating p-type conduction. The delafossite structure is comprised of alternating layers of slightly distorted edge-shared BO_6 octahedra and two-dimensional close-packed A-cation planes forming linear $O-A^{1+}-O$ "dumbbells",[3−5] as found in the well-known p-type oxide semiconductor Cu_2O.[6,7] Furthermore, the oxygens are coordinated by four cations (one A^{+1} and three B^{3+}). Depending on the stacking of the layers, two polytypes are possible. The "3R" polytype (Figure 1) consists of "AaBbCcAaBbCc..." stacking along the *c*-axis and has rhombohedral symmetry with the space group $R\bar{3}m$ (No. 166), whereas the "2H" polytype consists of an alternate stacking sequence ("AaBbAaBb...") and has the space group $P6_3/mmc$ (No. 194).[8]

$CuAlO_2$ exhibits small polaron conduction, a diffusion-limited conduction mechanism in which trapped holes and resultant lattice distortions "hop" between Cu-sites,

* To whom correspondence should be addressed. E-mail: t-mason@northwestern.edu.
† Current Address: ESRF, Grenoble Cedex, France.
‡ Current Address: Rubicon Technology, Inc., Franklin Park, IL 60131.
§ Current Address: Université Paul Sabatier Toulouse, Toulouse Cedex 4, France.

(1) Kawazoe, H.; Yanagi, H.; Ueda, K.; Hosono, H. *MRS Bull.* **2000**, *25* (8), 28−36.
(2) Kawazoe, H.; Yasukawa, M.; Hyodo, H.; Kurita, M.; Yanagi, H.; Hosono, H. *Nature* **1997**, *389*, 939−942.
(3) Prewitt, C. T.; Shannon, R. D.; Rogers, D. B. *Inorg. Chem.* **1971**, *10* (4), 719−723.
(4) Shannon, R. D.; Rogers, D. B.; Prewitt, C. T. *Inorg. Chem.* **1971**, *10* (4), 713−718.
(5) Köhler, B. U.; Jansen, M. *Z. Anorg. Allg. Chem.* **1986**, *543*, 73−80.
(6) Anderson, J. S.; Greenwood, N. N. *Proc. Royal Soc. London* **1952**, *215* (1122), 353−370.
(7) Young, A. P.; Schwartz, C. M. *J. Phys. Chem. Solids* **1969**, *30*, 249−252.

10.1021/cm048983c CCC: $27.50
Published on Web 12/02/2004

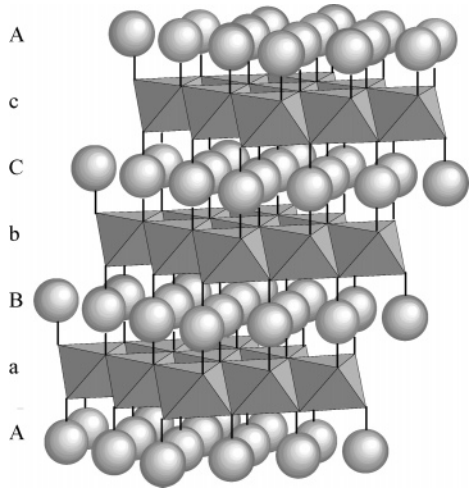

Figure 1. Schematic representation of the delafossite structure (ABO_2) for the "3R" polytype ($R\bar{3}m$) with AaBbCcAa... stacking along the *c*-axis. The "2H" polytype ($P6_3/mmc$) has an alternate AaBbAa... stacking sequence. The polyhedron and spheres represent BO_6 distorted octahedron and linearly coordinated A^{1+} cations, respectively.

which limits the room-temperature mobility to <1 $cm^2\ V^{-1}\ s^{-1}$.[9] Despite rather constant mobility values, conductivity values have been reported for $CuAlO_2$ between 1.7×10^{-3} and 17 S/cm corresponding to widely varying hole concentrations between 7.0×10^{16} and $1.2 \times 10^{20}\ cm^{-3}$.[1,10−16] Previous reports suggest the hole content in $CuAlO_2$, as well as in other delafossite compounds, is set by Cu-vacancies[17] or oxygen interstitials (especially in large B-site cation compounds, i.e., $CuYO_2$).[18] The defect chemistry of delafossite materials, however, is still not completely understood. The current paper (Part 1) focuses on the defect structure leading to hole generation in $CuAlO_2$ as it relates to two separate synthesis routes: high-temperature solid-state synthesis and low-temperature hydrothermal synthesis. Part 2[19] focuses on the transport and defect mechanisms in larger B-site cation delafossites: $CuScO_2$ and $CuYO_2$.

Experimental Procedure

Bulk polycrystalline samples for this study were produced by conventional high-temperature solid-state (SS) reactions. A reproducible process was found to produce single-phase $CuAlO_2$. High-purity constituent oxides (Adrich Chemical Co., Milwaukee, WI; 99.999−99.9999%) were mixed in proper stoichiometric ratios in an agate mortar and pestle under acetone. To ensure accurate molar proportion, the component oxides were dried in a furnace at 400 °C for 12 h and stored in a desiccator. Once a homogeneous mixture was obtained, pellets were uniaxially pressed at ~175−400 MPa. The pressed pellets were then surrounded by a small amount of sacrificial powder of the same nominal composition to prevent reaction between the pellet and the crucible. The pellets were heated in air to 1100 °C for 24−36 h and quench-cooled in air. This process of firing was repeated until an X-ray phase-pure sample of $CuAlO_2$ was achieved, which typically took two firing cycles. The percent theoretical density was estimated from the weight and geometric dimensions of the fired pellets and was typically 60−70% for all samples.

A low-temperature hydrothermal (HT) technique was used to synthesize powders of $CuAlO_2$,[20] similar to that first published by Shannon et al.[4] employing a FEP (fluoro-(ethylene-propylene)) Teflon pouch technique adapted from the work of Harrison et al.[21] Appropriate amounts of aluminum metal, copper oxides, and aluminum oxide were placed along with ground NaOH pellets in each FEP pouch. Mole fractions of the reactants were varied in accordance with the following reaction:

$$\phi CuO + {}^1/_2(1-\phi)Cu_2O + {}^1/_3\phi Al + {}^1/_6(3-\phi)Al_2O_3 \xrightarrow{NaOH} CuAlO_2 \quad (1)$$

The stoichiometric coefficients for this reaction represent the reduction of Cu^{II} to Cu^{I} and the oxidation of Al^0 to Al^{III}. The pouches were sealed and placed in an autoclave with deionized water. The autoclave was sealed and heated to an initial temperature of 150 °C to allow the H_2O to enter the permeable membrane of the pouch and dissolve the NaOH. The autoclave was then heated to 210 °C, and subsequently cooled to room temperature. Upon removal from the autoclave, each pouch contained both solid products, including CuO and Cu_2O, and excess solution. Owing to unreacted Cu_2O and CuO, which were evidenced for all values of ϕ in eq 1, the initial Cu sources were decreased (e.g., approximately 40% for $\phi = 0.33$) to yield phase-pure $CuAlO_2$.

Room- and high-temperature electrical and thermopower measurements, as described by Hong et al.,[22] were used to investigate the defect chemistry and transport mechanisms of bulk ceramic pellets. As mentioned previously, SS−$CuAlO_2$ samples were typically between 60 and 70% dense, and conductivity measurements were corrected for porosity using the Bruggeman symmetric medium equation as described by McLachlan et al.:[23]

$$\sigma_{measured} = \sigma_{actual}\,[1 - {}^3/_2 f] \quad (2)$$

where f is the volume fraction of porosity (valid for $0 \le f < 0.4$). Density corrections were found to increase the measured conductivity by a factor of 1.8 to 2.5. Thermopower values were converted to hole concentrations based on small polaron theory[24,25] as per the following equation:

$$Q = +\frac{k_B}{e}\ln\left(\frac{\beta(1-c)}{c}\right) \quad (3)$$

where k_B is Boltzmann's constant, e is the unit of electronic charge, the spin degeneracy factor (β) is typically 2, and c is

(8) Staehlin, W.; Oswald, H. R. *Z. Anorg. Allg. Chem.* **1970**, *373* (1), 69−72.
(9) Ingram, B. J.; Mason, T. O.; Asahi, R.; Park, K. T.; Freeman, A. J. *Phys. Rev. B* **2001**, *64* (15), 155114-1−15114-7.
(10) Benko, F. A.; Koffyberg, F. P. *J. Phys. Chem. Solids* **1984**, *45* (1), 57−59.
(11) Stauber, R. E.; Perkins, J. D.; Parilla, P. A.; Ginley, D. S. *Electrochem. Solid State Lett.* **1999**, *2* (12), 654−656.
(12) Gong, H.; Wang, Y.; Luo, Y. *Appl. Phys. Lett.* **2000**, *76* (26), 3959−3961.
(13) Gao, S.; Zhao, Y.; Gou, P.; Chen, N.; Xie, Y. *Nanotechnology* **2003**, *14*, 538−541.
(14) Wang, Y.; Gong, H. *Chem. Vap. Deposition* **2000**, *6* (6), 285−288.
(15) Lee, M. S.; Kim, T. Y.; Kim, D. *Appl. Phys. Lett.* **2001**, *79* (13), 2028−2030.
(16) Ohashi, M.; Iida, Y.; Morikawa, H. *J. Am. Ceram. Soc.* **2002**, *85* (1), 270−272.
(17) Katayama-Yoshida, H.; Koyanagi, T.; Funashima, H.; Harima, H.; Yanase, A. *Solid State Commun.* **2003**, *126*, 135−139.
(18) Cava, R. J.; Zandbergen, H. W.; Ramirez, A. P.; Takagi, H.; Chen, C. T.; Krajewski, J. J.; Peck, W. F., Jr.; Waszczak, J. V.; Meigs, G.; Roth, R. S.; Schneemeyer, L. F. *J. Solid State Chem.* **1993**, *104*, 437−452.
(19) Ingram, B. J.; Harder, B. J.; Hrabe, N. W.; Mason, T. O.; Poeppelmeier, K. R. *Chem. Mater.* **2004**, *16*, 5623−5629.
(20) Shahriari, D. Y.; Barnabe, A.; Mason, T. O.; Poeppelmeier, K. R. *Inorg. Chem.* **2001**, *40*, 5734−5735.
(21) Harrison, W. T. A.; Nenoff, T. M.; Gier, T. E.; Stucky, G. D. *Inorg. Chem.* **1993**, *32*, 2437−2441.
(22) Hong, B.-S.; Ford, S. J.; Mason, T. O. *Key Eng. Mater.* **1997**, *125−126*, 163−186.
(23) McLachlan, D. S.; Blaszkiewicz, M.; Newnham, R. E. *J. Am. Ceram. Soc.* **1990**, *73* (8), 2187−2202.

the fraction of sites occupied by holes $(Cu^{2+}_{Cu^{1+}})^{\bullet}$, such that the hole concentration, p, is given by cN, where N is the concentration of atomic sites (i.e., the Cu-site density in $CuAlO_2$ is 2.51×10^{22} cm^{-3}). At high temperature, thermal equilibrium was established by monitoring the time-dependence of in situ electrical properties.

The electrical conductivity of HT-$CuAlO_2$ powders was obtained by the powder−solution−composite (PSC) method, which compares the conductivity of an electrolyte/powder composite-slurry to that of the plain electrolyte using effective medium theory and impedance spectroscopy. The details are described elsewhere.[26]

Structural refinements of both HT- and SS-$CuAlO_2$ samples were performed using the Rietveld method. For the HT-$CuAlO_2$ sample, the general structure analysis system (GSAS)[27] software package was used. The data for the SS-$CuAlO_2$ sample were analyzed with the program FullProf 2000.[28] Powder X-ray diffraction (XRD) patterns were obtained for $10° \leq 2\theta \leq 140°$ with a step size of 0.02° on a XDS 2000 4-circle diffractometer with solid-state detector (Scintag, Inc.). Neutron time-of-flight (TOF) spectra were obtained from the special environment powder diffractometer (SEPD) located at the intense pulsed neutron source (IPNS) at Argonne National Lab (ANL).[29] The TOF data were collected from three detector banks located at 144.845°, 90°, and 44°.

Cation ratios were determined by inductively coupled plasma atomic emission spectroscopy (ICP). Selected samples for ICP were prepared by thoroughly dissolving approximately 0.1 g of $CuAlO_2$ in 25.0 mL of HNO_3. The resultant solution was diluted by a factor of 25 with deionized H_2O and subsequently analyzed with a Thermo Jarrell Ash Atomscan model 25 Sequential ICP spectrometer. Copper and aluminum emission peaks were evaluated at 324.754 and 308.215 nm, respectively. Three readings were taken per sample and averaged. Thermogravimetric analysis (TGA) was performed to determine the oxygen content of selected samples. Approximately 0.1 g of material was reduced under flowing forming gas (4−7% H_2, balance N_2) in a thermogravimetric analyzer model 2950 (TA Instruments), and the weight loss was precisely determined. The resultant products were analyzed by XRD to verify that the following reaction occurred:

$$2Cu_{1+x}Al_{1+y}O_{2+\delta} + (1 + 2\delta - 3y)H_{2(g)} \rightarrow 2(1 + x)Cu_{metal} + (1 + y)Al_2O_3 + (1 + 2\delta - 3y)H_2O_{(g)} \quad (4)$$

Results and Discussion

The properties of $CuAlO_2$ produced by two techniques, low-temperature hydrothermal (HT) and conventional high-temperature solid-state (SS) synthesis, were compared to gain an understanding of the defect mechanisms. HT-$CuAlO_2$ is predicted to possess enhanced electrical properties relative to SS-$CuAlO_2$ owing to nonequilibrium point defect populations.

Since the HT-$CuAlO_2$ powders could not be sintered into bulk ceramics without eliminating the hypothesized enhanced nonequilibrium defect populations, a powder−solution−composite (PSC) technique[26] was used to compare the electrical properties of HT- and SS-$CuAlO_2$. The electrical conductivity of multiple composite slurries comprised of $CuAlO_2$ powder and electrolytic solutions of varying strength (e.g., 0.001 M to 5.0 M NaCl) was determined with AC-impedance spectroscopy. The results were analyzed with effective medium theory and equivalent circuit modeling, and are shown in Figure 2. The Brueggeman asymmetric effective medium model[30] was fit to the conductivity values of the composite slurries (circles) and the powder's conductivity is determined where the conductivities of the composite and solution are equivalent (i.e., $\log(\sigma_{solution}/\sigma_{composite}) = 0$). From Figure 2 it is evident that the HT-$CuAlO_2$ exhibits approximately an order of magnitude increase in room-temperature conductivity over SS-$CuAlO_2$ (~0.2 and ~0.03 S/cm, respectively), which can be attributed to an increase in carrier concentration, as the mobility is expected to vary only slightly with hole concentration.

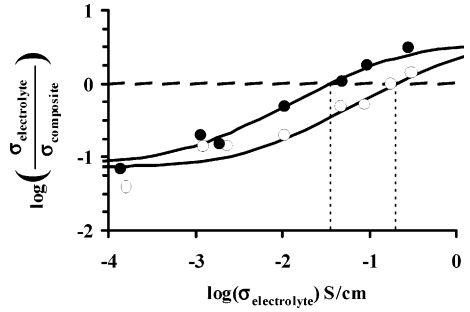

Figure 2. Comparison of HT-$CuAlO_2$ (closed circles) and SS-$CuAlO_2$ (open circles) powder−solution−composite conductivity measurements.[26] Conductivity estimate is given where the composite and electrolyte conductivities are equivalent (i.e., $\log(\sigma_{electrolyte}/\sigma_{composite}) = 0$).

Table 1. Tramp Impurity Survey of SS-$CuAlO_2$ Performed by Conam Kawin, Inc. using Test Method: ASTM E 663

impurity	concentration (ppm)
Cr	14
Ca	7
Mg	15
K	60
Fe	110
Na	310

The hole content of undoped SS-$CuAlO_2$ was determined by high-temperature thermopower measurements via eq 3 to be 3.0×10^{20} cm^{-3},[9] which compares favorably to the results of Gong et al.[12] and Yanagi et al.[31] As mentioned previously, several mechanisms have been suggested for hole generation, including extrinsic doping (or tramp impurities), oxygen interstitials, and cation vacancies. A tramp impurity survey performed on undoped SS-$CuAlO_2$ (Conam Kawin, Inc.) revealed several single and divalent cation impurities in small concentrations, as shown in Table 1, which could serve as acceptor dopants on the Al site (e.g., Ca_{Al}' or K_{Al}''). Summing the contribution of each tramp impurity, an upper bound of the hole concentration is found to be 1.2×10^{19} cm^{-3}. This value is believed to be an

(24) Tuller, H. L.; Nowick, A. S. *J. Phys. Chem. Solids* **1977**, *38*, 859−867.
(25) Ioffe, A. F. *Physics of Semiconductors*: Infosearch: London, 1960.
(26) Ingram, B. J.; Mason, T. O. *J. Electrochem. Soc.* **2002**, *150* (8), E396−E402.
(27) Larson, A. C.; Von Dreele, R. B. *General Structure Analysis System (GSAS)*; Los Alamos National Laboratory Report LAUR 86-748; Los Alamos, NM, 2000.
(28) Rodríguez-Carvajal, J. *FullProf 2000*; Laboratoire Léon Brillouin: Saclay, France, 2001. (http://www-llb.cea.fr/fullweb/winplotr/winplotr.htm).
(29) Jorgensen, J. D.; Faber, J., Jr.; Carpenter, J. M.; Crawford, R. K.; Haumann, J. R.; Hitterman, R. L.; Kleb, R.; Ostrowski, G. E.; Rotella, F. J.; Worlton, T. G. *J. Appl. Crystallogr.* **1989**, *22* (4), 321−333.
(30) Meredith, R. E.; Tobias, C. W. Conduction in Heterogeneous Systems. In *Advances in Electrochemistry and Electrochemical Engineering*; Tobias, C. W., Ed.; Interscience: New York, 1962.
(31) Yanagi, H.; Inoue, S.; Ueda, K.; Kawazoe, H.; Hosono, H.; Hamada, N. *J. Appl. Phys.* **2000**, *88* (7), 4159−4163.

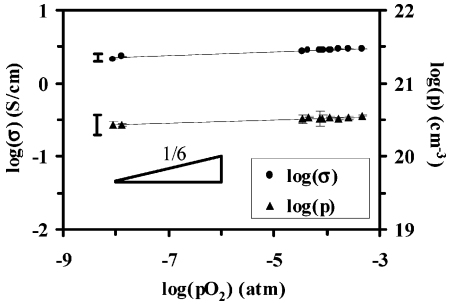

Figure 3. Oxygen dependence of the conductivity and hole concentration of SS-$CuAlO_2$ at 800 °C. Systematic error, consistent for each datum, is represented with error bars to the left, whereas random error is on the order of symbol size (or as indicated when larger). A $^1/_6$ log(pO_2)-dependence is shown for comparison.

overestimate owing to uncertainty in impurity defect site location and ionization (i.e., listed impurities are much larger than Al^{3+}) as well as typical over-estimation of Na content by ICP; nevertheless, it is an order of magnitude smaller than the experimentally determined hole content of 3.0×10^{20} cm^{-3}. It should be noted that Cr and Fe are expected to substitute for Al and should be in their trivalent oxidation state (isovalent with Al), and therefore should not contribute to hole generation. The above discussion suggests that tramp impurities are insufficient to account for the hole content found in $CuAlO_2$.

Excess oxygen contributions to hole generation were studied by varying pO_2 at constant temperature (800 °C) for SS-$CuAlO_2$ samples. The results are shown in Figure 3, in which the pO_2 dependence confirmed the overall p-type character of $CuAlO_2$ (i.e., conductivity increased slightly with increasing pO_2). The thermoelectric coefficient was positive (once again confirming p-type character) and virtually pO_2-independent. (The thermopower data are converted to hole concentrations in Figure 3, as per eq 3).

As seen in Figure 3, the hole concentration and conductivity of SS-$CuAlO_2$ exhibit significantly less than a $pO_2^{1/6}$ dependence. An intrinsic point defect mechanism, involving oxygen interstitials, such as

$$^1/_2O_{2(g)} \rightarrow O_i'' + 2h^\bullet \qquad (5)$$

is not the prevailing defect mechanism at 800 °C and $-8 < \log(pO_2) < -3$; otherwise, the hole concentration would depend on $pO_2^{1/6}$ (following eq 5)

$$\log(p) = constant + 1/6 \log(pO_2) \qquad (6)$$

This finding is consistent with the literature reporting little oxygen uptake in $CuAlO_2$.[10] Based on the Cu−Cu distance (a-lattice parameter) for $CuAlO_2$, the interstitial site available for excess oxygen has an approximate radius of 1.02 Å, which is small relative to an oxygen anion in 3-fold coordination (~1.22 Å),[32] thereby limiting the capacity for unbound oxygen interstitials.

The above findings indicate that neither aliovalent dopants nor oxygen-to-cation nonstoichiometry control the hole generation in $CuAlO_2$. Cation ratios in SS- and HT-CuAlO2 were verified with ICP analysis to investigate possible cation deficiencies. The variation from sample to sample was less than 2%. For SS-$CuAlO_2$, the average [Cu]/[Al] ratio was 0.96. The average [Cu]/[Al] ratio of 0.86 for HT-$CuAlO_2$ corresponds to a Cu/Al stoichiometry of 0.92:1.08, indicating the nonstoichiometric nature of the compound in favor of Al-excess. It should be noted that HT processing appears to produce a greater degree of nonstoichiometry than does the SS processing method. Furthermore, upon visual inspection of the two $CuAlO_2$ samples, a discrepancy in coloration is evident; the SS-$CuAlO_2$ exhibits a light blue-gray coloration whereas the HT-$CuAlO_2$ is gray-black, suggesting an increase in hole concentration. Solid-state specimens prepared with intentional Al-excess or Cu-excess showed little change in electrical properties relative to the nominally stoichiometric composition, when appropriately corrected for the presence of second phases, suggesting the solubility range of $CuAlO_2$ is small.

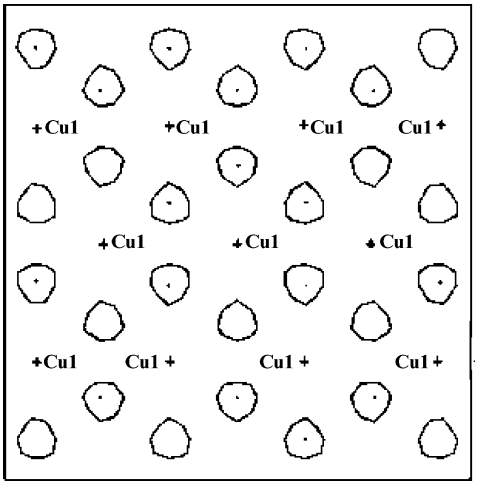

Figure 4. Fourier electron difference map of the (001) plane at $z = 0$ (Cu plane). The center of reference is located at 0 0 0 with a map size of 10×10 Å. Electron density contours are shown as lines and dots representing 0.21 and 0.42 electrons/Å^2, respectively. Refinement shows residual electron density when oxygen ions are not modeled on the 18*h* sites (centered between three Cu-ions).

To further establish the off-stoichiometric nature of $CuAlO_2$, structural refinements were performed on several $CuAlO_2$ samples. XRD diffraction data were collected for the HT-sample and refined with GSAS[29] in $R\bar{3}m$ using crystallographic data from previous refinements as a basis model.[5,33] It was assumed that all sites were fully occupied and thermal parameters were grouped by atom type and refined together. A good structural fit was found with a stoichiometric model; however, an electron density map of the basal plane revealed a significant amount of residual electron density that was unaccounted for in the regions surrounding the Cu ions, as seen in Figure 4.

To accurately determine the structure of HT-$CuAlO_2$, several models based on varying levels of nonstoichiometry and defect incorporation were used (e.g., V_{Cu}', O_i'', or $Al_{Cu}^{\bullet\bullet}$). Owing to the different X-ray scattering cross sections of Cu and Al, the occupation of a site by either of these ions can clearly be differentiated in a

(32) Shannon, R. D.; Prewitt, C. T. *Acta Crystallogr.* **1969**, *B25*, 925−946.

(33) Ishiguro, T.; Kitazawa, A.; Mizutani, N.; Kato, M. *J. Solid State Chem.* **1981**, *40*, 170−174.

Table 2. Crystallographic Parameters for HT- and SS-$CuAlO_2$ Based on Refinement of Powder Neutron TOF Data and/or XRD Data in the $R\bar{3}m$ Space Group

atom	site	x	y	z	B_{iso}	occupancy
				HT1-$CuAlO_2$ [a]		
Cu	3*a*	0	0	0	2.60(7) Å^2	0.925(8)
Al	3*a*	0	0	0	2.60(7) Å^2	0.075(8)
Al	3*b*	0	0	0.5	2.64(11) Å^2	1.000
O	6*c*	0	0	0.1097(2)	2.21(12) Å^2	1.000
O	18*h*	0.38(3)	−0.38(3)	−0.006(3)	2.21(12)Å^2	0.027(3)
				SS-$CuAlO_2$ [b]		
Cu	3*a*	0	0	0	β_{11}=0.04; β_{33}=0.00047	0.976(7)
Al	3*a*	0	0	0	β_{11}=0.04; β_{33}=0.00047	0.024(7)
Al	3*b*	0	0	0.5	β_{11}=0.022; β_{33}=0.00054	1.000
O	6*c*	0	0	0.10975(2)	0.68956 Å^2	1.000
O	36*i*	0.14(3)	0.00(3)	0.037(4)	0.68956 Å^2	0.0042(9)

[a] XRD, $\chi 2 = 1.77$: $R_p = 4.93\%$, $R_{wp} = 5.37\%$. $a = b = 2.8611(1)$ Å, $c = 16.9370(2)$ Å. [b] XRD: $R_p = 4.8\%$, $R_{wp} = 6.2\%$, $R_{exp} = 4.8\%$, and $R_{Bragg} = 7.1\%$. TOF (144.845°): $R_p = 5.0\%$, $R_{wp} = 5.3\%$, $R_{exp} = 3.0\%$, and $R_{Bragg} = 2.5\%$. TOF (90°): $R_p = 5.4\%$, $R_{wp} = 6.8\%$, $R_{exp} = 3.0\%$, and $R_{Bragg} = 2.0\%$. TOF (44°): $R_p = 3.7\%$, $R_{wp} = 3.7\%$, $R_{exp} = 5.4\%$, and $R_{Bragg} = 1.8\%$. $a = b = 2.85650(7)$ Å, $c = 16.9410(5)$ Å.

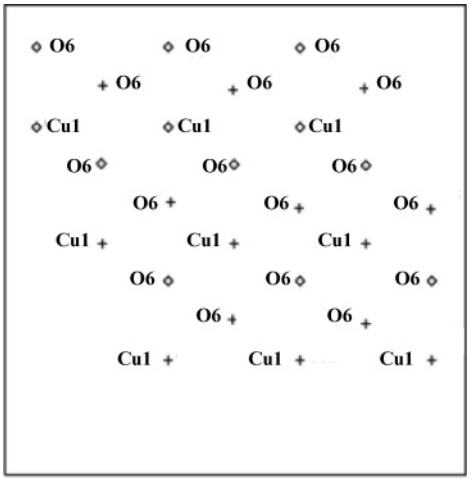

Figure 5. Fourier electron difference map of the (001) plane at $z = 0$ (Cu plane), with the center of reference located at 0 0 0 and a map size of 10 × 10 Å. Refinement shows no residual electron density when oxide ions are placed on the interstitial 18*h* sites (note: the 18*h* sites are only 2.7(3)% occupied as described in Table 2).

refinement. The model that produced the best fit revealed significant Al substitution on the Cu sites as well as interstitial oxygen. The final refinement cycle of this model yielded lattice parameters $a = b = 2.8611(1)$ Å, $c = 16.9370(2)$ Å, and $R_p = 4.93\%$, $R_{wp} = 5.37\%$, and $\chi^2 = 1.77$. The refinement values are presented in Table 2. An electron density map of the basal plane, shown in Figure 5, indicated that there is no residual electron density unaccounted for by this model. The Cu−O and $Al_{(octahedral)}$−O bond distances are 1.858(3) and 1.913(2) Å, respectively. These lengths were expected and matched those for previously reported samples of $CuAlO_2$.[5,33−35]

On the basis of the refined model, 7.5% excess Al ions occupy the copper (3*a*) sites in HT-$CuAlO_2$. In addition,

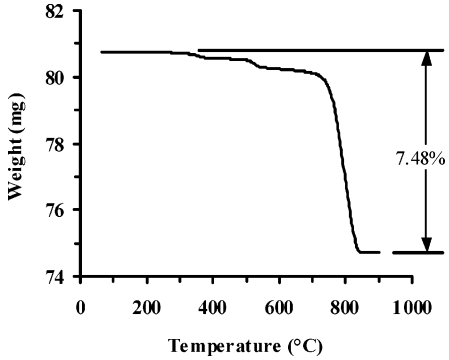

Figure 6. Thermogravemetric analysis results of $CuAlO_2$ reduction in 7% H_2/N_2 atmosphere. The final products (verified by PXRD) were Al_2O_3 and Cu metal.

0.162 extra oxide ions per formula unit were found on the interstitial 18*h* sites located within the two-dimensional Cu planes. A formula unit of $(Cu_{0.925(8)}Al_{0.075(8)})AlO_{2.162(18)}$ is therefore indicated for HT-$CuAlO_2$. TOF refinements of HT-$CuAlO_2$ showed reasonable agreement with the above results, however, the amount of available HT-powder (i.e., < 0.1 g per batch), was insufficient to obtain good fitting parameters.

Instead, the oxygen composition of HT-$CuAlO_2$ was experimentally verified by thermogravimetric analysis (TGA) as per eq 4, and the results are shown in Figure 6. A 7.48% weight loss is observed beginning at 325 °C. There are three weight loss steps, with the major step occurring between 750 and 850 °C. Infrared (IR) spectra of HT-$CuAlO_2$ did not reveal any excitations characteristic of O−H stretches. As such, the two low-temperature weight loss steps cannot be attributed to the loss of lattice water. Based on the final products, as characterized by XRD, and the level of weight loss, an initial oxygen content of 2.16 per formula unit was measured, consistent with the composition $(Cu_{0.925(8)}Al_{0.075(8)})AlO_{2.162(18)}$ as per the XRD data refinement.

The XRD and three TOF diffraction data sets collected on the SS-$CuAlO_2$ sample were combined and structurally refined using Rietveld analysis. The Debye−Waller factors were fixed to those obtained at 295 K by Ishiguro et al. using single crystals.[35] For the cation sites, anisotropic thermal parameters were used, while for the oxygen sites, the equivalent isotropic thermal parameter was calculated from the anisotropic values given in ref 35. The refinement indicated the presence of impurity phases: 1.3% $CuAl_2O_4$ and 1.9% 2H−$CuAlO_2$ with the balance 3R−$CuAlO_2$. The combined XRD/TOF refinement and relevant details for the 3R-polytype component are included in Table 2. The final refinement cycle yielded lattice parameters $a = b = 2.85650(7)$ Å, $c = 16.9410(5)$ Å. Owing to a broad local minimum between several refinement models and small defect populations, a precise defect determination was difficult to obtain from TOF/XRD refinements of SS-$CuAlO_2$, however the fit given in Table 2 was found to have the best parameters and is consistent with the previously discussed experimental observations, which are very sensitive to low defect populations. Unfortunately, TGA was unable to conclusively verify excess oxygen levels as is expected from the hole concentrations (determined from

(34) Ishiguro, T.; Ishizawa, N.; Mizutani, N.; Kato, M.; Tanaka, K.; Marumo, T. *Acta Crystallogr.* **1983**, *B39*, 564−569.
(35) Ishiguro, T.; Ishizawa, N.; Mizutani, N.; Kato, M. . *J. Solid State Chem.* **1982**, *41*, 132−137.

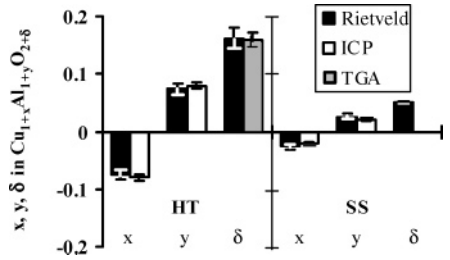

Figure 7. Review of off-stoichiometric levels as determined from structural refinements and gravimetric results in HT-$CuAlO_2$ (left side) and SS-$CuAlO_2$ (right side). Cu-deficiency and Al-excess in each sample are nearly equivalent and correspond to half the level of O-excess.

the thermoelectric coefficients) which suggests <0.02 oxygen excess per formula unit.

The above finding is intriguing since $Al_{Cu}^{\bullet\bullet}$ is a donor defect, which should produce n-type character instead of the experimentally determined p-type character of $CuAlO_2$. Furthermore, Al prefers higher coordination numbers than the Cu-site provides. A defect associate of the form $(Al_{Cu}^{\bullet\bullet}2O_i'')''$ is proposed, whereby two bound oxygen interstitials increase the coordination number of the Cu-site by forming a psuedo-tetrahedral site, thus stabilizing $Al_{Cu}^{\bullet\bullet}$ and accounting for the established excess oxygen. It should be noted that these oxygens are bound and nonresponsive to pO_2 changes at intermediate temperatures (as previously discussed). Agglomerations between these associates may exist, which would decrease the O_i'' to $Al_{Cu}^{\bullet\bullet}$ ratio. The refinement results have been verified by the TGA and ICP studies, supporting a 2:1 ratio between O_i'' and $Al_{Cu}^{\bullet\bullet}$ species in both HT-$CuAlO_2$ and SS-$CuAlO_2$. The hole concentration is therefore set by the Brouwer approximation at high temperatures

$$p \approx 2\,[(Al_{Cu}^{\bullet\bullet}2O_i'')''] \qquad (7)$$

leading to pO_2-independent electrical properties.

A carrier concentration of $1.2 \times 10^{21} \pm 0.35 \times 10^{21}$ cm^{-3} was obtained from eq 7 and the excess Al content listed in Table 2 for SS-$CuAlO_2$. A carrier concentration of $3.8 \times 10^{21} \pm 0.4 \times 10^{21}$ cm^{-3} is similarly obtained from the refinement values in Table 2 and eq 7 for HT-$CuAlO_2$, showing an increase in hole content relative to SS-$CuAlO_2$. The above results are reviewed in Figure 7 and show similar trends between the two synthesis routes, albeit on different scales. Both refinement and gravimetric studies demonstrate the Cu-deficiency and Al-excess levels are nearly equivalent and approximately half the level of O-excess, thereby supporting, in combination with electrical properties, the existence of $(Al_{Cu}^{\bullet\bullet}2O_i'')''$complexes.

It should be noted that the room-temperature thermopower of SS-$CuAlO_2$ was found to be ~670 μV/K, in agreement with Benko et al.[10] and significantly larger than the high-temperature value (~440 μV/K), suggesting a decrease in carrier content at low temperatures as per eq 3. This may be due to the trapping of mobile polarons (designated as $h^{\bullet}$) by the $(Al_{Cu}^{\bullet\bullet}2O_i'')''$ associates, as governed by the following equilibrium reaction:

$$2Cu_{Cu}^{\times} + (Al_{Cu}^{\bullet\bullet}2O_i'')'' + 2h^{\bullet} \leftrightarrow (Al_{Cu}^{\bullet\bullet}\,2O_i''\,2Cu_{Cu^{1+}}^{2+\bullet})^{\times} \qquad (8)$$

At elevated temperatures, the above equilibrium shifts to the left in favor of mobile holes; at room temperature, however, the equilibrium is shifted to the right, with a decrease in hole concentration.

Additional evidence for the trapping of mobile polarons with decreasing temperature as described by eq 8 is seen by comparing the hole concentrations at high and low temperatures with the change observed in the conductivity. On the basis of the thermoelectric values and eq 3, only ~ 7% of the carriers available for transport at high temperatures remain mobile at room temperature. The reduction in mobile holes is also seen in the reduced conductivity of SS-$CuAlO_2$ at room temperature (0.03 S/cm by PSC) vs high temperature (~3 S/cm in bar-specimens at 800 °C). Combining the high- and room-temperature hole content and conductivity values gives mobilities of 8.9×10^{-3} $cm^2\ V^{-1}\ s^{-1}$ and 6.2×10^{-2} $cm^2\ V^{-1}\ s^{-1}$ at room temperature and 800 °C, respectively. These mobility values correspond favorably with those calculated based on small polaron analysis:

$$\mu = g(1-c)ea^2\nu(k_BT)^{-1}\exp(-E_h/k_BT) \qquad (9)$$

where g is a geometric factor on the order of unity; c is the fraction of sites occupied by holes; a is the hopping distance (i.e., Cu−Cu distance), ν is the optical mode phonon frequency (~10^{13} s^{-1}); E_h is the hopping energy (~0.14 [9]), and k_B and e are Boltzman's constant and the charge on an electron, respectively. Given the character of the specimens in this study (loose powders or polycrystalline bars), independent measurements of room-temperature mobility were not possible.

Conclusions

Electrical property measurements, including high-temperature thermopower and conductivity, were compared with gravimetric studies and neutron time-of-flight and powder XRD refinements to establish a defect model for high-temperature solid state (SS) and low-temperature hydrothermal (HT) synthesized $CuAlO_2$.

Free oxygen interstitials were found to be minority species in SS-$CuAlO_2$ as evidenced by pO_2-independent conductivity and thermopower at 800 °C. Additionally, impurity levels (extrinsic doping) were insufficient to account for the observed hole concentrations in SS-$CuAlO_2$. In the absence of oxygen interstitials and extrinsic doping, the refinement and gravimetric results, reviewed in Figure 7, suggest that hole doping is governed by the intrinsic defect associate of the form $(Al_{Cu}^{\bullet\bullet}2O_i'')''$ which determines the hole population in $CuAlO_2$.

Comparison of electrical properties and site occupancies shows a significant difference in the off-stoichiometry observed between low-temperature hydrothermal and high-temperature solid-state synthesized compounds, leading to an order of magnitude increase in carrier content in HT-$CuAlO_2$. From these findings, it appears that the degree of off-stoichiometry in $CuAlO_2$ is synthesis-dependent, which may explain the large discrepancy in reported hole concentrations. It should be noted that although the hole content can be large at high-temperature, a significant fraction of holes become immobile at low-temperatures. Even at elevated tem-

peratures the mobility is limited by the small polaron conduction mechanism (<1 cm^2 V^{-1} s^{-1}) regardless of the synthesis route. Based on the hydrothermal method discussed in this paper, optimal synthesis techniques require a combination of low synthesis temperature and an intimate mixing of cation species. Not surprisingly, low-temperature techniques (i.e., sol−gel, hydrothermal, and various thin-film growth techniques) often lead to enhanced doping/defect levels, transport properties, and high carrier concentrations due to the nonequilibrium processes involved.

Acknowledgment. This work was supported in part under NSF-MRSEC grant DMR-9632472 and under DOE-NREL subcontract XAT-5-33636-02. Furthermore, the work at IPNS was supported by DOE W-31-1-0-ENG-38. Author B.J.I. was additionally supported through a NDSEG fellowship.

CM048983C